

Coulomb correlation effects in zinc monochalcogenides

S. Zh. Karazhanov

Department of Chemistry, University of Oslo, P.O. Box 1033 Blindern, N-0315 Oslo, Norway and

Physical-Technical Institute, 2B Mavljanov St., Tashkent, 700084, Uzbekistan

P. Ravindran, A. Kjekshus, and H. Fjellvåg

Department of Chemistry, University of Oslo, P.O. Box 1033 Blindern, N-0315 Oslo, Norway

U. Grossner and B. G. Svensson

Department of Physics, University of Oslo, P.O. Box 1048 Blindern, N-0316 Oslo, Norway

(Dated: June 22, 2021)

Electronic structure and band characteristics for zinc monochalcogenides with zinc-blende- and wurtzite-type structures are studied by first-principles density-functional-theory calculations with different approximations. It is shown that the local-density approximation underestimates the band gap and energy splitting between the states at the top of the valence band, misplaces the energy levels of the Zn-3d states, and overestimates the crystal-field-splitting energy. The spin-orbit-coupling energy is found to be overestimated for both variants of ZnO, underestimated for ZnS with wurtzite-type structure, and more or less correct for ZnSe and ZnTe with zinc-blende-type structure. The order of the states at the top of the valence band is found to be anomalous for both variants of ZnO, but is normal for the other zinc monochalcogenides considered. It is shown that the Zn-3d electrons and their interference with the O-2p electrons are responsible for the anomalous order. The effective masses of the electrons at the conduction-band minimum and of the holes at the valence-band maximum have been calculated and show that the holes are much heavier than the conduction-band electrons in agreement with experimental findings. The calculations, moreover, indicate that the effective masses of the holes are much more anisotropic than the electrons. The typical errors in the calculated band gaps and related parameters for ZnO originate from strong Coulomb correlations, which are found to be highly significant for this compound. The local-density-approximation with multiorbital mean-field Hubbard potential approach is found to correct the strong correlation of the Zn-3d electrons, and thus to improve the agreement between the experimentally established location of the Zn-3d levels and that derived from pure LDA calculations.

PACS numbers: 71.15.-m ; 71.22.+i

I. INTRODUCTION

Wide band-gap semiconductors are very important for applications in optical devices such as visual displays, high-density optical memories, transparent conductors, solid-state laser devices, photodetectors, solar cells etc. The functional usefulness of such devices of the zinc monochalcogenides depends on electronic properties at the point at the valence-band (VB) maximum and conduction-band (CB) minimum (recalling that these compounds have direct band gaps). Therefore, first-principles calculations for these compounds are of considerable importance.

Up to now, most ab initio studies have been based on the density-functional theory (DFT)¹ in the local-density approximation (LDA).² For many materials, the theory provides a good description of ground-state properties. However, problems arise when the DFT/LDA approach is applied to materials with strong Coulomb correlation effects,^{3,4,5} traceable back to the mean-field character of the Kohn-Sham equations as well as to the poor description of strong Coulomb correlation and exchange interaction between electrons in the narrow band. One of the problems is that the LDA error in calculation of the band gap becomes larger than the common LDA error. Several attempts have been made to include the correlation effects in the DFT/LDA calculations. The LDA plus self-interaction correction (LDA+ SIC)^{6,7,8,9,10} eliminates the spurious interaction of an electron with itself as occurring in the conventional DFT/LDA. This approach has been widely used to study compounds with completed semicore-d shells,^{7,8,9,10,11,12} and it is found to lower the Zn-3d levels derived from the simple LDA, thus giving better agreement with the measured X-ray emission spectra (XES) and effective masses of carriers.^{7,8,9,12} The calculated value of the band gap (E_g) then falls within the established error limits for the LDA.^{7,8,9,10,13}

Another promising approach for correlated materials is the so-called LDA plus multiorbital mean-field Hubbard potential (LDA+U),^{3,4,5} which includes the on-site Coulomb interaction in the LDA Hamiltonian. After adding the on-site Coulomb interaction to the L(S)DA Hamiltonian, the potential becomes spin and orbital dependent. The LDA+U, although being a mean-field approach, has the advantage of describing both the chemical bonding and the electron-electron interaction. The main intention of the LDA+U approach is to describe the electronic interactions of strongly correlated states. Such a computational procedure is widely used to study materials with ions that contain incomplete d or f shells, e.g., transition-metal oxides, heavy fermion systems etc.^{3,4,5} Recently, such approach has been applied to ZnO^{14,15,16,17} with completed semicore-Zn-3d valence shell. However, it is concluded in Refs. 15,16 that LDA+U calculations, in principle, should not have improved the size of the E_g because the Zn-3d bands are located well below the Fermi level (E_F).

Despite the required large sized computations, different versions of the GW approximation^{18,19} have also been used

to study zinc monochalcogenides.^{20,21,22,23} (G stands for one-particle Green's function as derived from many-body perturbation theory and W for Coulomb screened interactions.) This approximation can take into account both non-locality and energy-dependent features of correlations in many-body system and can correctly describe excited-state properties of a system by including its ionization potential and electron affinity. Band-structure studies using the the GW correction show that E_g is underestimated by 1.2 eV for ZnO,²⁰ by 0.53 eV for ZnS,²¹ and by 0.55 eV for ZnSe.²¹ However, the GW calculations in Ref. 22 overestimated E_g for ZnO by 0.84 eV. Recent studies²⁴ of Zn, Cd, and Hg monochalcogenides by the GW approach has shown that the band-gap underestimation is in the range 0.3{0.6 eV. Incorporation of the plasmon pole model for screening has lead to systematic errors. Combination of exact exchange (EXX) DFT calculations in the optimized-effective-potential approach with GW is found²³ to give better agreement with the experimental band gaps and the location of the Zn-3d levels. Recently, excellent agreement with experiment was achieved by all-electron full-potential EXX calculations²⁵ for locations of the d bands for a number of semiconductors and insulators (Ge, GaAs, CdS, Si, ZnS, C, BN, Ne, Ar, Kr, and Xe), although the band gap was not as close to experimental data as found in other pseudopotential EXX calculations.

Despite intense studies, many of the fundamental properties of these materials are still poorly understood and further experimental and theoretical studies are highly desirable. One target is the so-called eigenvalue problem. For example, LDA underestimates E_g for ZnO,^{15,16,17,20,22} ZnS,²¹ and ZnSe,²¹ by more (in fact by > 50 %) than expected for a typical LDA error. Also, the actual positions of the Zn-3d levels,^{15,16,17,20,21,22} the band dispersion, crystal-field splitting (ϵ_{CF}), and spin-orbit coupling splitting (ϵ_{SO})^{7,17} are not reproduced correctly. Neither the use of the generalized-gradient approximation (GGA) nor the inclusion of SO coupling into the calculations seems able to remedy the above shortcomings.^{15,17,26}

The effective masses of the charge carriers are more indefinite parameters for the zinc monochalcogenides. Owing to low crystal quality only a few cyclotron resonance experiments have been performed for ZnO,^{27,28} ZnS,^{29,30} and ZnTe.³¹ The status for the present situation is that effective masses from different ab initio packages and experiments scatter appreciably in publications on ZnO (Refs. 7,27,28,30,32,33,34) and ZnTe (Refs. 29,31,35).

In this work zinc monochalcogenides (ZnX ; X = O, S, Se, Te) in the zinc-blende-(z-) and wurtzite-(w-)type structural arrangements are studied by first-principles calculations within the LDA, GGA, and LDA+U approaches with and without SO coupling.

II. COMPUTATIONAL DETAILS

The electronic band structure of the ZnX z - and w -phases is studied using the VASP (PAW) package³⁶, which calculates the Kohn-Sham eigenvalues within the framework of DFT.¹ The calculations have been performed with the use of the LDA,² GGA,³⁷ and simplified rotationally invariant LDA + U^{3,4} approaches. The exchange- and correlation-energy per electron have been described by the Perdew-Zunger parametrization³⁸ of the quantum Monte Carlo procedure of Ceperley-Alder.³⁹ The interaction between electrons and atomic cores is described by means of non-normal-conserving pseudopotentials implemented in the VASP package.³⁶ The pseudopotentials are generated in accordance with the projector-augmented-wave (PAW) method.^{40,41} For the PAW method, high-precision energy cutoffs have been chosen for all the ZnX phases considered. The use of the PAW pseudopotentials addresses the problem of the inadequate description of the wave functions in the core region common to other pseudopotential approaches.⁴² The application allows us to construct orthonormalized all-electron-like wave functions for the Zn-3d, 4s and anion-s and p -valence electrons of the zinc monochalcogenides under consideration.

Self-consistent calculations were performed using a $10 \times 10 \times 10$ mesh frame according to Monkhorst-Pack scheme for z -type structures and a similar density of k points in the Γ -centered grids for w -type phases. The completely filled semicore-Zn-3d states have been considered as valence states.

For band-structure calculations we used the experimentally determined crystal-structure parameters (Table I) for all phases considered. The ideal positional parameter u for X in the w -type structures is calculated on the assumption of equal nearest-neighbor bond lengths:³²

$$u = \frac{1}{3} \frac{a}{c} + \frac{1}{4} \quad (1)$$

The values of u for the ideal case agree well with the experimental values u_{Expt} (see Table I). The unit-cell vectors of the z -type structures are $a = (0; 1=2; 1=2)a$; $b = (1=2; 0; 1=2)a$; $c = (1=2; 1=2; 0)a$, a is the cubic lattice constant, and there are four ZnX formula units per unit cell specified by Zn at $(0; 0; 0)$ and X at $(1=4; 1=4; 1=4)$. In the w -type structure, the lattice vectors are $a = (1=2; \frac{c}{3}=2; 0)a$; $b = (1=2; \frac{c}{3}=2; 0)a$; $c = (0; 0; c=a)a$, c/a is the axial ratio, and there are two ZnX formula units per hexagonal unit cell, Zn at $(0; 0; 0)$ and $(2=3; 1=3; 1=2)$ and X at $(0; 0; u)$ and $(2=3; 1=3; u + 1=2)$.

The values of the U and J parameters were calculated within the constrained DFT theory.⁵¹ Furthermore, the position of the Zn-3d bands was calculated as a function of U using the LDA + U method, and U was derived empirically on forcing match to the experimentally established⁵² location of the Zn-3d bands. The thus obtained empirical

values of U were used to explore further the electronic structure within the LDA + U procedure.

Values of ϵ_{CF} , ϵ_{SO} , and the average band gap E_0 for ZnO (with anomalous order of the states at the top of the VB) are calculated from the expressions:^{53,54}

$$E_0 = \frac{1}{3} (E_g(A) + E_g(B) + E_g(C)) \quad (2)$$

$$\epsilon_{CF} = \frac{1}{2} (\epsilon_{CB} + \epsilon_{BA} + \frac{\epsilon_{CA}^2 + \epsilon_{BA}^2 + \epsilon_{CB}^2}{3}) \quad (3)$$

where $E_g(A)$; $E_g(B)$; and $E_g(C)$ are energy gaps determined from ab initio calculations and $\epsilon_{CB} = E_g(C) - E_g(B)$; $\epsilon_{BA} = E_g(B) - E_g(A)$, and $\epsilon_{CA} = E_g(C) - E_g(A)$. To calculate these parameters for the other ZnX phases, and for ZnO with normal order of the states at the top of the VB, ϵ_{CB} and ϵ_{CA} in Eq. 3 have been exchanged.

For investigation of the order of the states at the top of the VB for ZnO in z- and w-type structural arrangements, band-structure calculations have been performed using the MINDLAB package,⁵⁵ which uses the full potential linear minimization orbital (FP-LMTO) method, and by the WIEN2K code,⁵⁶ which is based on a full-potential linearized-augmented plane-wave method.

III. RESULTS AND DISCUSSIONS

A. The electronic structure at the top of VB

Important optical and transport properties for semiconductors are determined by the carriers close to $k = 0$ in the vicinity of the Γ point. The VB spectrum near the Γ point is different for z- and w-type materials. Without SO coupling the top of the VB for phases with w-type structure is split into a doublet ϵ_5 and a singlet ϵ_1 state by the crystal field (Fig.1). The ϵ_5 is a $p_x; p_y$ -like state, while ϵ_1 is a p_z -like state. Inclusion of SO coupling gives rise to three twofold degenerate bands in the VB, which are denoted as hh (heavy holes), lh (light holes), and sh (spin-split-off holes) (Fig.1). These states correspond to A, B, and C exciton lines in photoluminescence experiments.⁵⁴ The symmetry of two of these three bands are of Γ_7 character and one of Γ_9 character. The Γ_7 state derived from ϵ_5 will obtain a slight admixture of p_z while Γ_9 stays unmixed p_x and p_y like. For ZnO, these bands calculated within LDA, GGA, and LDA + U for $U < 9.0$ eV, are in the order of decreasing energy Γ_7 ; Γ_9 , and Γ_7 , which is referred to as anomalous order, resulting from a negative ϵ_{SO} .⁵⁷ For $U > 9.0$ eV the lower Γ_7 state interchanges with Γ_9 , so the order becomes Γ_7 ; Γ_7 , and Γ_9 . For the other ZnX-w phases the sequence is Γ_9 ; Γ_7 ; Γ_7 , named as normal order,⁵⁸ and the order was not changed by LDA + U . Without SO coupling the VB spectrum near the Γ point for the ZnX-z phases

originates from the sixfold degenerate Γ_6 state. The SO interaction splits the Γ_6 level into fourfold degenerate Γ_8 (hh and lh) and doubly degenerate Γ_7 (sh) levels.

B. Band structure

Initial band-structure calculations have been performed for ZnO-w using three different pseudopotentials for the oxygen atom supplied with the VASP package: ordinary, soft, and high-accuracy oxygen pseudopotentials. Band dispersion, band gaps $[E_g; E_g(A); E_g(B); E_g(C); \text{and } E_0]$, E_{CF} , and E_{SO} corresponding to these oxygen pseudopotentials do not differ significantly from each other and the subsequent calculations were performed using the ordinary oxygen pseudopotential.

Band-parameter values calculated with or without taking SO couplings into consideration are listed in Table II. Band gaps and the mean energy level of Zn-3d electrons E_d from LDA calculations are underestimated, while E_{CF} is overestimated compared to the experimental data. The DFT-LDA error is quite pronounced for ZnO compared to the other ZnX phases and the discrepancy exceeds the usual error for LDA calculations. The discrepancies in the calculated E_{CF} values for ZnO compared to experimental values are unacceptably large. Except for ZnO, the calculated E_{CF} values within the different approaches do not differ much, emphasizing that Coulomb correlation effects are more pronounced for ZnO than ZnS, ZnSe, and ZnTe.

The calculations show (Table II) that E_{SO} is much smaller than 1.0 eV for all phases except ZnSe-z ($E_{SO} = 0.40$ eV) and ZnTe-z ($E_{SO} = 0.97$ eV). The SO coupling energy calculated for ZnO-z and -w within LDA and GGA, is negative, while it is positive for the other ZnX phases. The numerical value of E_{SO} calculated within the three approaches considered came out close to each other for all ZnX phases. The numerical value of E_{SO} is severely underestimated for ZnO-w and ZnS-w compared to experimental data. Our E_{SO} values for the other ZnX-z phases in Table II are in good agreement with theoretical calculations⁶¹ by the LAPW method and the available experimental data.

C. Density of states

Analysis of the density of states (DOS) for the ZnX phases (Fig. 2), calculated within the LDA, shows that the Zn-3d states are inappropriately close to the CB, which contradicts the findings from XPS, XES, and UPS experiments.^{52,62,63} Furthermore, these states and the top of the VB are hybridized. Distinct from the other ZnX phases considered, ZnO in both z- and w-type structure shows artificially widened Zn-3d states. These discrepancies

indicate strong Coulomb correlation between narrow Zn-3d states which is not accounted for correctly in the LDA calculations. As a consequence, the interactions of the semicore-Zn-3d states with O-2p in VB are artificially enlarged, the band dispersions are falsified, the widths of the O-p and Zn-3d bands are altered, and the latter are shifted inappropriately close to the CB. These findings indicate that correlation effects of the Zn-3d states should be taken into account to obtain a more proper description of the electronic structure for the ZnX phases, especially for the z- and w-type variants of ZnO.

The simplified rotationally invariant LDA+U approach^{3,4} has been used to correct the strong correlation of the Zn-3d electrons. This approach uses U and J to describe the strong Coulomb correlation, but since these parameters do not explicitly take into account the d-orbital state, we did not regard the regular LDA+U approach as sufficiently rigorous, and we therefore rather preferred empirically assigned U and J values. For comparison, the values of U and J have been calculated for some of the compounds within the constrained DFT⁵¹ (Table III), showing that the calculated values to some extent agrees with those extracted empirically.

Using the empirical values for the parameters U and J , band-structure calculations have been performed within LDA+U. Figure 3 shows the dependence of the Zn-3d mean level (E_d) and E_g of the ZnX phases on U . A analysis of the illustrations show that the LDA+U-derived band gaps are more reasonable than the pure LDA-derived band gaps (see also Table II). Moreover, the deviation of the E_g values obtained using LDA+U from those obtained by experiments are much smaller than those calculated using the pure LDA (Fig. 2 and Table II).

The values of the peaks in the DOS (Fig. 2), corresponding to the Zn-3d states calculated by the LDA+U, are much larger than those calculated using the pure LDA. This indicates that according to the LDA+U the semicore-Zn-3d electrons become more localized than according to the pure LDA. Distinct from the other ZnX phases considered, the width of the Zn-3d bands for ZnO calculated by LDA+U become much narrower than that calculated by LDA (Fig. 2). However, LDA+U only slightly changed the width of the Zn-3d bands of the other ZnX phases, which leads one to conclude that the Coulomb correlation effects for ZnO is more pronounced than for the other compounds considered.

D. Order of states at the top of VB

The order of states at the top of VB in ZnO-w is a frequently debated topic at present (see, e.g., Refs. 7,65,66). The present project has addressed this problem for the ZnX phases by LDA, GGA, and LDA+U calculations within the VASP, MINDLAB, and WIEN2K packages with and without including the SO couplings. The results obtained by

LDA and LDA+U within VASP are presented in Figs. 4 and 5. By inspection of the degeneracy of the eigenvalues it is found that the normal order $\epsilon_5 > \epsilon_1$ of the states at the top of VB is obtained by LDA without SO coupling for all ZnX-w phases. The same order was obtained by calculations within GGA. However, upon using the LDA+U approach with the semiempirical values for the parameter U (Table III) the order of the states at the top of VB for the ZnO-w is changed, while there appears no changes for the other ZnX phases.

The variations in the order of the states at the top of the VB on U are systematically studied for the ZnO-z (Fig. 6) and ZnO-w (Fig. 7) phases, with and without including SO coupling. It is found that at $U = 9.0$ eV, the LDA+U without SO coupling interchanges the sequence of the VB states from $\epsilon_5 > \epsilon_1$ to $\epsilon_1 > \epsilon_5$.

Since one can treat the semi-core-Zn-3d electrons as core electrons and freeze their interaction with VB in theoretical calculations, we studied the VB structure of ZnO using the MindLab package⁵⁵ including the semi-core-Zn-3d electrons in the core. On this assumption one obtains the order $\epsilon_1 > \epsilon_5$ at the top of the VB for ZnO-w. Hence, the order of the states in this case can be traced back to the treatment of the Zn-3d electrons. On comparing the structures at the top of the VB calculated within the LDA and GGA approaches it is found that only quantitatively small changes have occurred. Hence, inhomogeneities in the electron gas do not affect the order of the states at the top of VB, and only slightly change the band dispersion.

On the involvement of the SO coupling, the ϵ_5 and ϵ_1 states of ZnO-w are split into two ϵ_7 and one ϵ_9 states (see Fig. 1). Orbital decomposition analysis was performed to establish the origin and order of these states using the band structure calculated according to the WIEN2K package.⁵⁶ The order of the states was found to be $\epsilon_7 > \epsilon_9 > \epsilon_7$ (LDA, GGA, and LDA+U ($U < 9.0$ eV) calculations), viz. "anomalous" order.^{7,32,57,67,68}

The above analysis shows that among the ZnX phases considered, ZnO are most sensitive to Coulomb correlation effects. The values for c_F extracted from the $\epsilon_5\{\epsilon_1$ splitting according to the LDA without SO coupling are positive and decrease with increasing U (Fig. 8). Correspondingly, c_{SO} obtained on including the SO coupling came out negative and increased in size with increasing U. The order of the states is in this case anomalous ($\epsilon_7 > \epsilon_9 > \epsilon_7$), thus supporting findings according to the model of Thomas (see Refs. 7,32,57,67,68).

At high values of U (> 9.0 eV), c_F becomes negative, which indicates inversion from $\epsilon_5 > \epsilon_1$ to $\epsilon_1 > \epsilon_5$ in the order of the states at the top of VB without the SO coupling. Upon inclusion of the SO coupling the order becomes $\epsilon_7 > \epsilon_7 > \epsilon_9$, which does not agree with either of the two models for the order of states. At present the safest conclusion is that the parameter U takes a value below 9.0 eV and that the order of the states at the top of VB consequently must be classified as anomalous.

The variation of the energy splitting of the A;B; and C states, expressed by $E_A - E_B$; $E_A - E_C$; and $E_B - E_C$; in the VB for ZnO-z and -w as a function of U is displayed in Fig. 8. For values of U below 9.0 eV the energy splitting decreases with increasing U. At higher values of U; $E_A - E_B$ becomes negative and decreases, $E_B - E_C$ increases, while $E_A - E_C$ stays more or less constant.

Distinct from ZnO-w, the other ZnX-w phases exhibit a normal order of the states at the top VB ($\epsilon_5 < \epsilon_1$ and $\epsilon_7 < \epsilon_7 < \epsilon_9$ without and with the SO coupling, respectively). This order does not change upon variation of the value of U in the LDA+U calculations.

Without introduction of the SO coupling, the top of the VB for the ZnX-z phases is triple degenerate (see Figs. 1 and 5). When the SO coupling is included in the consideration, the VB maximum is split in fourfold (ϵ_8) and twofold (ϵ_7) states with the normal $\epsilon_8 > \epsilon_7$ order for X = S, Se, and Te. However, the order is anomalous for ZnO-z ($\epsilon_7 > \epsilon_8$) and in addition ϵ_{SO} becomes negative. The dependence of ϵ_{SO} on U is shown in Fig. 10, revealing that for U > 8.0 eV ϵ_{SO} becomes positive, and consequently that normal order is restored for the states at the top of VB. So, one can ascribe the anomalous order of the states at the top of VB in ZnO-z to Coulomb correlation effects related to the Zn-3d electrons.

For all cases considered, the GGA approximation did not influence the order. Hence, inhomogeneities in the distribution of the electron gas do not play a significant role for the order of the states at the top of VB.

IV. EFFECTIVE MASSES

The CB states with short wave vectors ($k = 0$) are doubly degenerate with respect to spin and can be characterized by one or two energy-independent effective masses for the z- and w-type arrangements. The effective masses are calculated along the directions $\Gamma - A$; $\Gamma - M$, and $\Gamma - K$ within the LDA, GGA, and LDA+U approaches with and without including the SO couplings (Tables IV and V). According to the conventional notations carrier effective masses for the ZnX-z phases are distinguished by the indices e, hh, lh, and sh, sh corresponding to ϵ_1 , and hh and lh to ϵ_5 . The carrier masses for the ZnX-w phases are distinguished by the indices e, A, B, and C.

The calculated m_e for the ZnX-z phases are more isotropic than those for the ZnX-w phases. The numerical values of m_e for ZnO-w, ZnS-w, ZnSe-z, and ZnTe-z obtained by the LDA are underestimated by about 50% compared to experimental findings,^{27,28,29,33} while those for the other ZnX phases agree fairly well with experimental data. GGA and LDA+U calculations only slightly improved the LDA-derived m_e values for all ZnX phases except ZnO, whereas the latter showed much better agreement with LDA+U. This indicates once again that correlation effects are more

pronounced for ZnO than for the other phases considered.

The electron effective mass is smaller along the direction $\Gamma - A(k)$ than along $\Gamma - M(?)$ and $\Gamma - K(?)$. This feature can be important in $\Gamma - M$ and superlattice constructions of these phases.³⁰ The heavy holes along all directions (see Tables IV and V) and light holes along the $\Gamma - A(k)$ direction are much heavier than other holes and, in particular, CB electrons. For example, the carrier transport in ZnO is dominated by electrons, while that by holes can in practice be ruled out. This in turn explains the experimentally established large disparity²⁹ between electron and hole mobilities, and also may explain the large optical non-linearity in ZnO.³⁰ The effective masses of the holes are more anisotropic than those of electrons, which can be traced back to states at the top of VB associated with O p orbitals, and this can give rise to anisotropy in parameters like carrier mobility.⁶⁹

On comparison of the m_e values in Tables IV and V one sees that the influence of SO coupling on m_e is very important for ZnSe-z and ZnTe-z, while for the other phases its effect is small. The present values for ZnO are in reasonable agreement with the experimental values,^{27,28,29,33} except for m_A^k ; m_B^k , and $m_C^?$ (the latter discrepancies being not understood) and in good agreement with those obtained⁷ by the FP-LMTO method.

V. CONCLUSIONS

Electronic structure and band characteristics for ZnX -z and -w phases are studied by first-principles calculations within the LDA, GGA, and LDA+U approaches. It is found that LDA underestimates the band gaps, the actual positions of the energy levels of the Zn-3d states, and splitting energies between the states at the top of the valence band, but overestimates the crystal-field splitting energy. Spin-orbit coupling energy is overestimated for ZnO -w, underestimated for ZnS -w, and comes out more or less accurate for ZnS -z, ZnSe -z, and ZnTe -z.

The LDA+U approach has been used to account properly for the strong correlation of the Zn-3d electrons. The value of the Hubbard U potential was varied to adjust the Zn-3d band derived from LDA toward lower energies and thus provide better agreement with the experimentally established location of the Zn-3d levels from X-ray emission spectra. Using the U values obtained by this approach the calculated band gaps and band parameters are improved according to the LDA+U procedure compared to the pure LDA approach.

The order of the states at the top of the valence band is systematically examined for ZnX phases. It is found that the ZnO -z and -w phases exhibit negative SO splitting and anomalous order of the states within LDA, GGA, and LDA+U for $U < 9.0$ eV, and the model of Thomas^{7,32,57,67} is supported for these two ZnX phases. It is found that in the LDA+U calculations the anomalous order is maintained up to $U = 8.0$ eV for ZnO -z and $U = 9.0$ eV for ZnO -w. For values of U above these limits, the order is inverted. For ZnO -w, ϵ_{CF} goes from positive to negative,

whereas s_0 converts to a complex quantity, and becomes thus meaningless. Based on these analyses it is concluded that the Zn-3d electrons are responsible for the anomalous order of the states at the top of the valence band in ZnO. In the other ZnX phases considered, the order is normal for all values of U used in the calculations. For the three approaches considered, our findings confirm the model of Thomas⁶⁷ regarding the order of the states in the valence band of ZnO.

Effective masses of electrons at the conduction band minimum and of holes at the valence band maximum have been calculated along the symmetry axis M ; A , and K for the w-type phases and along X ; K , and L for the z-type phases. Along the c axis of the w-type phases the light- and heavy-hole bands are degenerate, but the degeneracy is broken when spin-orbit coupling is included. The heavy holes in the valence band are found to be much heavier than the conduction band electrons in agreement with experimental findings which show higher electron mobility than hole mobility. The calculations, moreover, reveal that effective masses of the holes are much more anisotropic than those of the electrons. Conduction band electron masses for ZnO-w, ZnS-w, ZnSe-z, and ZnTe-z calculated within LDA are underestimated by about 50% compared to experimental data, while those for the other ZnX phases are considered to agree with experimental data.

The GGA approach did not remedy the DFT-LDA derived error in the calculated energy gaps and band parameters. We found that spin-orbit coupling is important for calculation of the parameters for ZnSe-z and ZnTe-z, while it is not significant for the other zinc monochalcogenides.

It should be noted that electronegativity difference (according to the Pauling scale) 1.9 for ZnO is much larger than 0.9, 0.8, and 0.5 for ZnS, ZnSe, and ZnTe, respectively, which reflects that ZnO is more ionic than the other ZnX compounds. Consequently, our calculated DOS for the topmost valence band is relatively narrow for ZnO, which accordingly shows stronger correlation effects than the other ZnX.

It is established that the unusually large errors in calculated (according to DFT within LDA) band gaps and band parameters are owing to strong Coulomb correlations, which are found to be most significant in ZnO among the ZnX phases considered. Also, because of the increase in ionic radii of X with increasing atomic number the Zn-X bond length systematically increases from ZnO to ZnTe. As a result, the Zn-3d band moves toward lower energies (see Fig. 2) and behaves like core electrons. In contrast, the relatively short Zn-O distance further confirms that the interaction of the Zn-3d electrons with the valence band is stronger in ZnO than in the other ZnX compounds. Consistent with the above view point, the Zn-3d band of ZnO-w and ZnO-z is located closer to the topmost valence band, thus increasing the influence of the Coulomb correlation effects to the electronic structure compared to the

other ZnX_{-w} and ZnX_{-z} phases. The present conclusion is consistent with the results in Ref. 25, which report that locations of the d bands of a number of semiconductors and insulators (Ge, GaAs, CdS, Si, ZnS, C, BN, Ne, Ar, Kr, and Xe), determined from all-electron full-potential exact-exchange-DFT calculations, are in excellent agreement with experiment.

Acknowledgments

This work has received financial and supercomputing support from FUNMAT. SZK has obtained partial financial support from the Academy of Sciences of Uzbekistan (Project N 31-36). SZK also thanks R. Vidya, P. Vajstoon, and A. K. Laveness (Department of Chemistry, University of Oslo, Oslo, Norway) for discussions and assistance. The authors thank Professor M. A. Korotin (Institute of Metal Physics, Ekaterinburg, Russia) for help with the computations of the values of the parameters U and J within the constrained DFT and Dr. Karel Kizek (Institute of Physics ASCR, Prague, Czech Republic) for assistance with calculations according to the WIEN2K package.

-
- ¹ P. Hohenberg and W. Kohn, *Phys. Rev.* **136**, B 864 (1964).
 - ² W. Kohn and L. J. Sham, *Phys. Rev.* **140**, A 1133 (1965).
 - ³ V. I. Anisimov, I. V. Solovyev, M. A. Korotin, M. T. Czyzyk, and G. A. Sawatzky, *Phys. Rev. B* **48**, 16 929 (1993).
 - ⁴ S. L. Dudarev, G. A. Botton, S. Y. Savrasov, C. J. Humphreys, and A. P. Sutton, *Phys. Rev. B* **57**, 1505 (1998).
 - ⁵ O. Bengone, M. Alouani, B. Bichl, and J. Hugel, *Phys. Rev. B* **62**, 16 392 (2000).
 - ⁶ A. Svane and O. Gunnarsson, *Phys. Rev. Lett.* **65**, 1148 (1990).
 - ⁷ W. R. L. Lambrecht, A. V. Rodina, S. Limpijumnong, B. Segall, and B. K. Meyer, *Phys. Rev. B* **65**, 07 5207 (2002).
 - ⁸ D. Vogel, P. Krüger, and J. Polmann, *Phys. Rev. B* **52**, 14 316 (1995).
 - ⁹ D. Vogel, P. Krüger, and J. Polmann, *Phys. Rev. B* **54**, 5495 (1996).
 - ¹⁰ C. L. Dong, C. Persson, L. Vayssieres, A. Augustsson, T. Schmitt, M. Matesini, R. Ahuja, C. L. Chang, and J.-H. Guo, *Phys. Rev. B* **70**, 19 5325 (2004).
 - ¹¹ A. Qteish, *J. Phys.: Condens. Matter* **12**, 5639 (2000).
 - ¹² C. Persson and A. Zunger, *Phys. Rev. B* **68**, 07 3205 (2003).
 - ¹³ B. K. Agrawal, P. S. Yadav, and S. Agrawal, *Phys. Rev. B* **50**, 14 881 (1994).
 - ¹⁴ A. Janotti and C. G. Van de Walle, *J. Cryst. Growth* **287**, 58 (2006).
 - ¹⁵ M. S. Park and B. I. Min, *Phys. Rev. B* **68**, 22 4436 (2003).
 - ¹⁶ X. Feng, *J. Phys.: Condens. Matter* **16**, 4251 (2004).
 - ¹⁷ S. Zh. Karazhanov, P. Ravindran, U. Grossner, A. Kjekshus, H. Fjellvag, and B. G. Svensson, *J. Cryst. Growth* **287**, 162 (2006).
 - ¹⁸ L. Hedin, *Phys. Rev.* **139**, A 796 (1965).
 - ¹⁹ M. S. Hybertsen and S. G. Louie, *Phys. Rev. Lett.* **55**, 1418 (1985).
 - ²⁰ M. Ueda, N. Hamada, T. Kotani, and M. Schilfgaarde, *Phys. Rev. B* **66**, 12 5101 (2002).
 - ²¹ W. Luo, S. Ismail-Beigi, M. L. Cohen, and S. G. Louie, *Phys. Rev. B* **66**, 19 5215 (2002).
 - ²² M. Oshikiri and F. Aryasetiawan, *J. Phys. Soc. Jpn.* **69**, 2113 (2000).
 - ²³ P. Rinke, A. Qteish, J. Neugebauer, C. Freysoldt, and M. Scheer, *arXiv:cond-mat/0502404* **1**, 1 (2005).
 - ²⁴ A. Fleszar and W. Hanke, *Phys. Rev. B* **71**, 045207 (2005).
 - ²⁵ S. Shama, J. K. Dewhurst, and C. Ambrosch-Deraxl, *Phys. Rev. Lett.* **95**, 136402 (2005).
 - ²⁶ J. E. Jaffe, J. A. Snyder, Z. Lin, and A. C. Hess, *Phys. Rev. B* **62**, 1660 (2000).
 - ²⁷ Y. Imamura, M. Oshikiri, K. Takehana, T. Takamasu, and G. Kido, *Physica B* **298**, 211 (2001).
 - ²⁸ M. Oshikiri, K. Takehana, T. Asano, and G. Kido, *Physica B* **216**, 351 (1996).

- ²⁹ Data in Science and Technology. Semiconductors: Other than Group IV Elements and III-V Compounds, edited by O. Madelung (Springer, Berlin, 1992).
- ³⁰ Y.-N. Xu and W.-Y. Ching, *Phys. Rev. B* **48**, 4335 (1993).
- ³¹ B. Clerjaud, A. Gelineau, D. Galland, and K. Saminadayar, *Phys. Rev. B* **19**, 2056 (1979).
- ³² L.C. Lew Yan Voon, M. Willatzen, and M. Cardona, *Phys. Rev. B* **53**, 10 703 (1996).
- ³³ K. Hummer, *Phys. Status Solidi B* **56**, 249 (1973).
- ³⁴ M. Oshikiri, F. Aryasetiawan, Y. Imataka, and G. Kido, *Phys. Rev. B* **66**, 12 5204 (2002).
- ³⁵ R.E. Nahory and H.Y. Fan, *Phys. Rev. B* **156**, 825 (1967).
- ³⁶ G. Kresse and J. Furthmüller, *Phys. Rev. B* **54**, 11 169 (1996).
- ³⁷ J.P. Perdew, K. Burke, and M. Ernzerhof, *Phys. Rev. Lett.* **77**, 3865 (1996).
- ³⁸ J.P. Perdew and A. Zunger, *Phys. Rev. B* **23**, 5048 (1981).
- ³⁹ D.M. Ceperley and B.J. Alder, *Phys. Rev. Lett.* **45**, 566 (1980).
- ⁴⁰ P.E. Blochl, *Phys. Rev. B* **50**, 17 953 (1994).
- ⁴¹ G. Kresse and D. Joubert, *Phys. Rev. B* **59**, 1758 (1999).
- ⁴² B. Adolph, J. Furthmüller, and F. Bechstedt, *Phys. Rev. B* **63**, 12 5108 (2001).
- ⁴³ Inorganic Crystal Structure Database (Gmelin Institut, Karlsruhe, 2001).
- ⁴⁴ Handbook of Laser Science and Technology, vol. III, edited by M.J. Weber (CRC, Cleveland, 1986).
- ⁴⁵ O. Zakharov, A. Rubio, X. Blase, M.L. Cohen, and S.G. Louie, *Phys. Rev. B* **50**, 10 780 (1994).
- ⁴⁶ N. Lakshmi, N.M. Rao, R. Venugopal, D.R. Reddy, and B.K. Reddy, *Mater. Chem. Phys.* **82**, 764 (2003).
- ⁴⁷ V.N. Tomashik, G.S. Oleinik, and I.B. Mizetskaya, *Inorg. Mater.* **14**, 1119 (1978).
- ⁴⁸ W.H. Bragg and J.A. Darbyshire, *J. Met.* **6**, 238 (1954).
- ⁴⁹ Numerical Data and Functional Relationships in Science and Technology, vol. 17a and 22a of Landolt-Börnstein, New series. Group III, edited by K.H. Hellwege and O. Madelung (Springer, New York, 1982).
- ⁵⁰ CRC Handbook of Chemistry and Physics, 70th ed., edited by R.C. Weast, D.R. Lide, M.J. Astle, and W.H. Beyer (Chemical Rubber, Boca Raton, 1990).
- ⁵¹ W.E. Pickett, S.C. Erwin, and E.C. Ethridge, *Phys. Rev. B* **58**, 1201 (1998).
- ⁵² M. Ruckh, D. Schmid, and H.W. Schock, *J. Appl. Phys.* **76**, 5945 (1994).
- ⁵³ J.J. Hopfeld, *J. Phys. Chem. Solids* **15**, 97 (1960).
- ⁵⁴ A. Mang, K. Reinann, and S. Rubenacke, *Solid State Commun.* **94**, 251 (1995).
- ⁵⁵ S.Y. Savrasov, *Phys. Rev. B* **54**, 16470 (1996).
- ⁵⁶ P. Blaha, K. Schwarz, G. Madsen, D. Kvasnicka, and J. Luitz, *WIEN2K, An Augmented Plane-Wave + Local Orbitals Program for Calculating Crystal Properties* (Techn. Universität Wien, Austria, 2001).

- ⁵⁷ J. E. Rowe, M. Cardona, and F. H. Pollak, *Solid State Commun.* **6**, 239 (1968).
- ⁵⁸ D. G. Thomas and J. J. Hopfeld, *Phys. Rev.* **116**, 573 (1959).
- ⁵⁹ *Numerical Data and Functional Relationships in Science and Technology. New Series. Group III: Crystal and Solid State Physics. Semiconductors. Supplements and Extensions to Volume III/17. Intrinsic Properties of Group IV Elements and III{V, II{V I and I{V II Compounds*, vol. 22a, edited by O. Madelung and M. Schulz (Springer, Berlin, 1982).
- ⁶⁰ Y. Zidon, J. Yang, and Y. Shapira, *Appl. Phys. Lett.* **81**, 436 (2002).
- ⁶¹ P. Carrier and S. H. Wei, *Phys. Rev. B* **70**, 035212 (2004).
- ⁶² L. Ley, R. A. Pollak, F. R. McFeely, S. P. Kowalczyk, and D. A. Shirley, *Phys. Rev. B* **9**, 600 (1974).
- ⁶³ C. J. Vesely and D. W. Langer, *Phys. Rev. B* **4**, 451 (1971).
- ⁶⁴ *Numerical Data and Functional Relationships in Science and Technology*, vol. 22a of Landolt-Bornstein, New series. Group III, edited by K. H. Hellwege and O. Madelung (Springer, Berlin, 1987).
- ⁶⁵ D. C. Reynolds, D. C. Look, B. Jogai, C. W. Litton, G. Cantwell, and W. C. Harsch, *Phys. Rev. B* **60**, 2340 (1999).
- ⁶⁶ D. C. Reynolds, D. C. Look, B. Jogai, and T. C. Collins, *Appl. Phys. Lett.* **79**, 3794 (2001).
- ⁶⁷ D. G. Thomas, *J. Phys. Chem.* **15**, 86 (1960).
- ⁶⁸ K. Shindo, A. Morita, and H. Kamimura, *J. Phys. Soc. Jpn.* **20**, 2054 (1965).
- ⁶⁹ B. Santic, *Semicond. Sci. Technol.* **18**, 219 (2003).

TABLE I: Experimentally determined unit-cell dimensions a ; c , volumes (V), and ideal (u ; calculated by Eq. 1) and experimental ($u_{\text{E x p t}}$) positional parameters for the X atom of the w -type phases. For w -type structures $a = b$. For z -type structures $a = b = c$ and all atoms are in fixed positions.

Phase	a (Å)	c (Å)	V (Å ³)	$u_{\text{E x p t}}$	u
ZnO- w^a	3:250	5:207	47:62	0:3825	0:3799
ZnS- w^b	3:811	6:234	78:41	0:3750	0:3746
ZnSe- w^c	3:996	6:626	91:63	0:3750	0:3712
ZnTe- w^d	4:320	7:100	114:75	0:3750	0:3734
ZnO- z^e	4:620		98:61		
ZnS- z^f	5:409		158:25		
ZnSe- z^g	5:662		181:51		
ZnTe- z^g	6:101		227:09		

^aExperimental value from Ref. 43.

^bExperimental value from Refs. 30,44.

^cExperimental value from Refs. 43,45.

^dExperimental value from Refs. 46,47.

^eExperimental value from Ref. 48.

^fExperimental value from Refs. 49,50.

^gExperimental value from Refs. 13,50.

TABLE II: Band gaps [E_g ; $E_g(A)$; $E_g(B)$; $E_g(C)$; and E_0], crystal field (${}^0_{CF}$; ${}_{CF}$), and spin-orbit (${}_{SO}$) splitting energies (all in eV) for ZnX phases with w- and z-type structures calculated within LDA, GGA, and LDA+U approaches. E_g and ${}^0_{CF}$ refer to calculations without SO coupling, in all other calculations the SO interactions are accounted for. Experimental values are quoted when available.

Phase	Method	E_g	$E_g(A)$	$E_g(B)$	$E_g(C)$	E_0	E_d	${}^0_{CF}$	${}_{CF}$	${}_{SO}$
ZnO-w	LDA	0.744	0.724	0.756	0.839	0.773	5.00	0.095	0.093	-0.043
	GGA	0.804	0.783	0.817	0.900	0.833	5.00	0.097	0.094	-0.044
	LDA+U	1.988	2.008	2.053	2.053	2.038	10.00			
	Expt. ¹		3.441	3.443	3.482	3.455			0.039	-0.004
ZnS-w	LDA	1.990	1.968	1.995	2.073	2.012	6.50	0.069	0.052	0.027
	GGA	2.232	2.211	2.236	2.310	2.253	6.00	0.066	0.049	0.025
	LDA+U	2.283	2.260	2.286	2.366	2.304	8.20	0.059	0.055	0.026
	Expt. ²		3.864	3.893	3.981				0.058	0.086
	Expt. ²		3.872	3.900				0.006	0.092	
ZnSe-w	LDA	1.070	0.939	1.008	1.379	1.109	6.50	0.114	0.324	0.047
	GGA	1.327	1.200	1.268	1.624	1.364	6.50	0.112	0.311	0.046
	LDA+U	1.404	1.271	1.334	1.721	1.442	9.30	0.101	0.347	0.041
	Expt. ³		2.860	2.876	2.926		9.20			
ZnTe-w	LDA	1.052	0.760	0.820	1.691	1.091	7.50	0.086	0.838	0.033
	GGA	1.258	0.974	1.032	1.875	1.294	7.20	0.084	0.812	0.032
	LDA+U	1.283	0.990	1.043	1.882	1.305	9.50	0.075	0.809	0.030
	Expt. ⁴		2.260							
ZnO-z	LDA	0.573	0.555		0.588	0.577	4.60			-0.033
	GGA	0.641	0.615		0.649	0.638	4.60			-0.034
	LDA+U	1.486	1.495		1.497	1.496	7.90			0.002
	Empirical		3.300							
ZnS-z	LDA	1.875	1.852		1.916	1.873	6.10			0.064
	GGA	2.113	2.092		2.151	2.112	6.00			0.059
	LDA+U	2.332	2.310		2.389	2.336	9.00			0.079
	Expt. ²		3.680		3.740		9.00			0.067

Continued on next page

TABLE II: { continued from previous page

Phase	Method	E_g	$E_g(A)$	$E_g(B)$	$E_g(C)$	E_0	E_d	$^0_{CF}$	CF	so
	Expt. ²		3.780		3.850					
ZnSe-z	LDA	1.079	0.948		1.341	1.079	6.60			0.393
	GGA	1.335	1.209		1.586	1.335	6.50			0.377
	LDA+U	1.421	1.291		1.700	1.427	9.05			0.409
	Expt. ²		2.700				9.20			0.400
	Expt. ²		2.820							0.400
ZnTe-z	LDA	1.061	0.772		1.668	1.070	7.10			0.897
	GGA	1.267	0.986		1.853	1.275	7.05			0.867
	LDA+U	1.329	1.046		1.956	1.349	9.90			0.911
	Expt. ²		2.394				9.84			0.970
	Expt. ²						10.30			

¹ Experimental value from Ref. 54.

² Experimental value from Ref. 59.

³ Experimental value from Refs. 29,59.

⁴ Experimental value from Ref. 60.

TABLE III: Values of U and J calculated within the constrained DFT⁵¹ for ZnX -w phases and extracted within LDA+U by fitting the energy level of Zn-3d electrons to band locations from XPS, XES, and UPS experiments.^{52,62,63} Calculations have not been performed for the z- ZnX phases within the constrained DFT.

Method		ZnO-w	ZnS-w	ZnSe-w	ZnTe-w	ZnO-z	ZnS-z	ZnSe-z	ZnTe-z
LDA+U	U	13.00	6.00	8.00	7.00	8.00	9.00	8.00	8.00
	J	1.00	1.00	0.91	0.89	1.00	1.00	0.91	1.00
Constrained DFT	U	11.10	9.74	9.33	7.00				
	J	0.91	0.90	0.91	0.89				

TABLE IV: Effective masses of electrons and holes (in units of the free-electron mass m_0) for ZnX-w calculated within LDA, GGA, and LDA+U approaches. The results are compared with the calculated and experimental data from Ref. 29 (directions not specified) and those calculated by FP-LMTO (Ref. 7), LCAO (Ref. 30) and determined experimentally (Ref. 33). Labelling of the effective masses is not changed with changed order of the states at the top of VB.

Phase	Method	m_e^k	$m_e^?$	m_A^k	$m_A^?$	m_B^k	$m_B^?$	m_C^k	$m_C^?$
Without SO coupling									
ZnO-w	LDA	0:139	0:132	2:943	2:567	2:943	0:150	0:157	3:476
	GGA	0:147	0:140	3:233	2:864	3:233	0:162	0:161	2:272
	LDA+U	0:234	0:221		4:770			3:750	0:266
ZnS-w	LDA	0:151	0:172	1:500	1:517	1:500	0:168	0:136	1:332
	GGA	0:158	0:184	1:589	1:611	1:589	0:177	0:151	1:201
	LDA+U	0:159	0:176	1:763	1:759	1:745	0:178	0:147	1:368
ZnSe-w	LDA	1:434	0:087	1:494	1:423	1:397	0:088		0:756
	GGA	0:093	0:105	1:386	1:327	1:386	0:105	0:086	1:068
	LDA+U	1:476	0:110	1:597	1:584	1:751	0:109	0:090	1:008
ZnTe-w	LDA	0:067	0:079	1:072	1:166	1:072	0:074	0:061	0:663
	GGA	0:078	0:092	1:073	1:089	1:063	0:088	0:070	0:751
	LDA+U	0:080	0:095	1:236	1:322	1:225	0:087	0:071	0:876
With SO coupling									
ZnO-w	LDA	0:137	0:130	2:447	2:063	2:979	0:227	0:169	0:288
	GGA	0:144	0:143	2:266	0:351	3:227	0:300	0:165	0:537
	LDA+U	0:189	0:209	0:207	11:401	4:330	3:111	0:330	0:270
	FP-LMTO ¹	0:230	0:210	2:740	0:540	3:030	0:550	0:270	1:120
	Expt. ²	0:24		0:590	0:590	0:590	0:590	0:310	0:550
	LCAO ³	0:280	0:320	1:980	4:310				
ZnS-w	LDA	0:144	0:153	1:746	3:838	0:756	0:180	0:183	0:337
	GGA	0:142	0:199	2:176	1:713	0:402	0:198	0:440	0:443
	LDA+U	0:138	0:157	1:785	2:194	0:621	0:195	0:339	0:303

Continued on next page

TABLE IV : { continued from previous page

Phase	Method	m_e^k	$m_e^?$	m_A^k	$m_A^?$	m_B^k	$m_B^?$	m_C^k	$m_C^?$
	Expt. ⁴	0:280		1:400	0:490				
	LCAO ³	0:260	0:330	1:510	1:470				
ZnSe-w	LDA	0:148	0:139	1:404	0:158	0:114	0:124	0:171	0:197
	GGA	0:184	0:149	1:395	0:184	0:135	0:173	0:190	0:306
	LDA+U	0:185	0:149	1:629	0:189	0:137	0:187	0:???	0:344
ZnTe-w	LDA	0:108	0:128	1:042	0:118	0:070	0:105	0:229	0:237
	GGA	0:134	0:182	1:044	0:122	0:102	0:145	0:239	0:246
	LDA+U	0:131	0:184	1:116	0:131	0:128	0:166		
	Expt. ⁴	0:130		0:600					

¹ Theoretical value from Ref. 7.

² Experimental value from Ref. 33.

³ Theoretical value from Ref. 30.

⁴ Experimental value from Ref. 29.

TABLE V: Effective masses of electrons and holes (in units of the free-electron mass m_0) for ZnX-z. The results are compared to calculated and experimentally determined data cited in Ref. 29. The labelling of the effective masses for ZnO-z has not been changed upon the change in the order of the states at the top of VB.

Phase	Method	m_e	m_{hh}^{100}	m_{hh}^{110}	m_{hh}^{111}	m_{lh}^{100}	m_{lh}^{110}	m_{lh}^{111}	m_{so}^{100}	m_{so}^{110}	m_{so}^{111}
Without SO coupling											
ZnO-z	LDA	0.110	1.400	5.345	2.738	1.400	1.436	2.738	0.120	0.114	0.112
	GGA	0.120	1.480	5.800	3.162	1.480	1.540	3.162	0.136	0.130	0.125
	LDA+U	0.193	1.780	8.041	3.820	1.780	1.727	3.820	0.224	0.202	0.198
ZnS-z	LDA	0.155	0.662	3.405	1.467	0.662	0.683	1.467	0.161	0.134	0.129
	GGA	0.172	0.710	3.800	1.500	0.710	0.710	1.500	0.188	0.145	0.155
	LDA+U	0.177	1.674	4.318		1.674	0.882		0.214	0.164	0.192
ZnSe-z	LDA	0.084	0.606	3.520	1.383	0.606	0.585	1.383	0.085	0.076	0.076
	GGA	0.100	0.626	3.430	1.320	0.626	0.600	1.320	0.106	0.090	0.090
	LDA+U	0.097	0.667		1.605	0.677	0.677	1.605	0.105	0.090	0.090
ZnTe-z	LDA	0.073	0.445	2.764	1.003	0.451	0.450	1.042	0.073	0.065	0.062
	GGA	0.085	0.440	2.701	1.046	0.443	0.452	1.044	0.086	0.075	0.072
	LDA+U	0.090	0.519	3.812	1.202	0.519	0.516	1.202	0.089	0.075	0.075
With SO coupling											
ZnO-z	LDA	0.110	0.390	0.571	0.385	1.520	1.100	1.330	0.174	0.164	0.169
	GGA	0.120	0.409	0.579	0.492	1.505	1.252	1.281	0.188	0.186	0.181
	LDA+U	0.193	1.782	2.920	1.972	0.968	1.392	1.669	0.250	0.240	0.230
ZnS-z	LDA	0.150	0.775	1.766	2.755	0.224	0.188	0.188	0.385	0.355	0.365
	GGA	0.172	0.783	1.251	3.143	0.233	0.216	0.202	0.378	0.373	0.383
	LDA+U	0.176	1.023	1.227	1.687	0.268	0.252	0.218	0.512	0.445	0.447
	Expt. ¹	0.184			1.760		0.230				
	Expt. ¹	0.340									
ZnSe-z	LDA	0.077	0.564	1.310	1.924	0.104	0.100	0.094	0.250	0.246	0.254
	GGA	0.098	0.568	0.922	1.901	0.126	0.122	0.111	0.271	0.273	0.267
	LDA+U	0.100	0.636	1.670	1.920	0.129	0.120	0.117	0.287	0.297	0.309

Continued on next page

TABLE V: { continued from previous page

Phase	Method	m_e^k	$m_e^?$	m_A^k	$m_A^?$	m_B^k	$m_B^?$	m_C^k	$m_C^?$		
	Expt. ¹	0:130	0:570	0:750							
	Expt. ¹	0:170									
ZnTe-z	LDA	0:064	0:381	0:822	1:119	0:071	0:067	0:066	0:254	0:253	0:256
	GGA	0:078	0:418	0:638	1:194	0:093	0:086	0:081	0:261	0:255	0:274
	LDA + U	0:081	0:483	0:929	1:318	0:096	0:088	0:085	0:288	0:292	0:290
	Expt. ¹	0:130		0:600							

¹ Experimental value from Ref. 29.

Figure 1

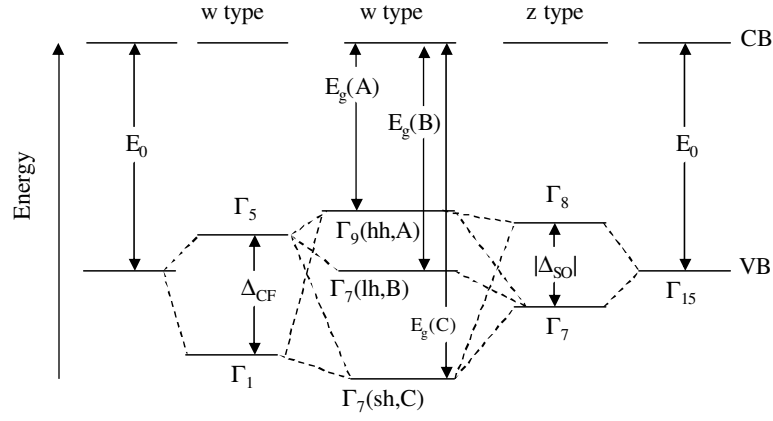


FIG. 1: Schematic representation of the band mixing in ZnX phases with z- and w-type structure. In w-type structures the levels Γ_9 , Γ_7 (upper), and Γ_7 (lower) are formed due to the combined influence (in the middle) of Δ_{CF} (on the left) and Δ_{SO} (on the right). In z-type phases the levels Γ_8 and Γ_7 are separated due to the SO interaction.

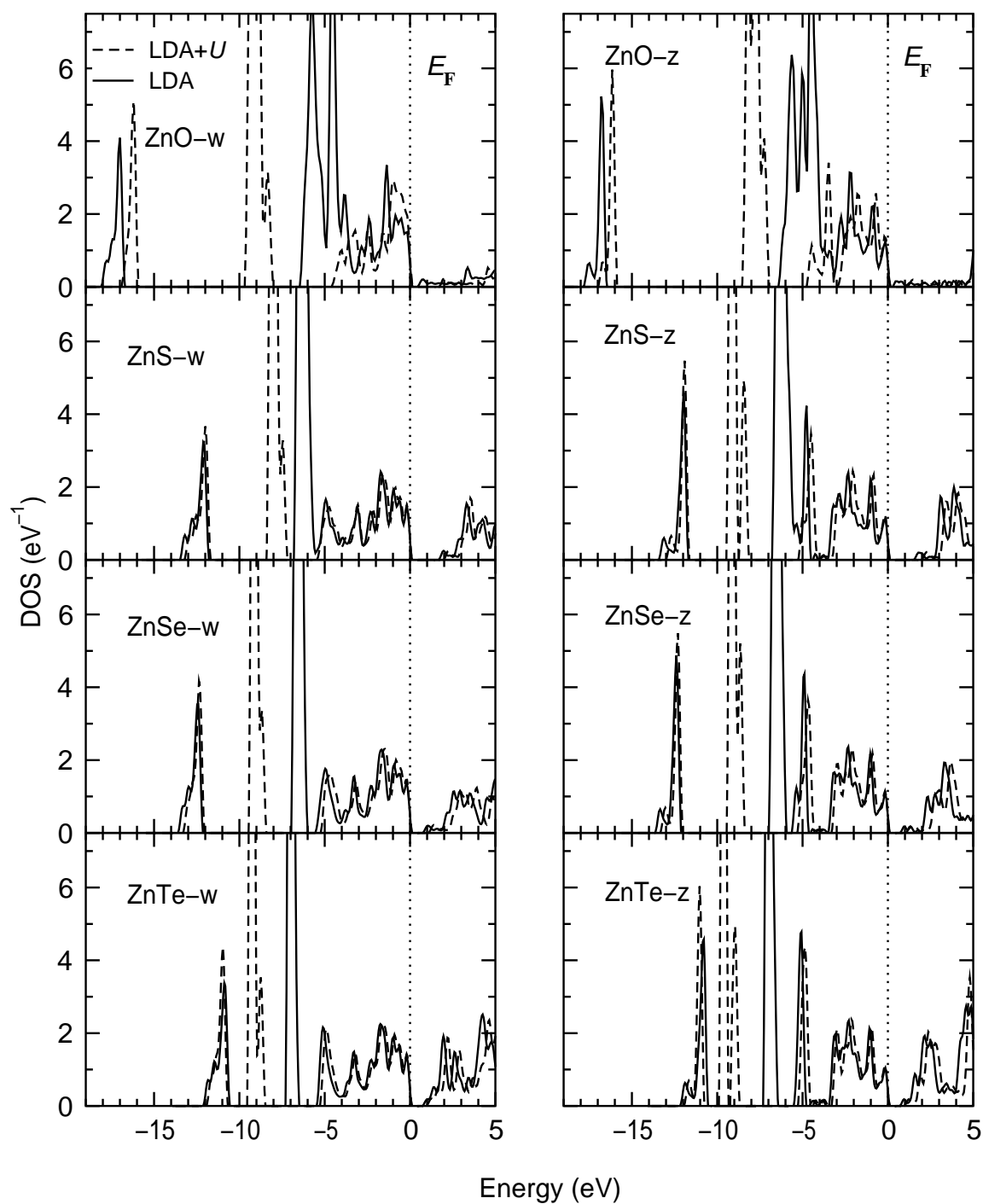


FIG . 2: Total density of states for ZnX -z and -w phases calculated from the LDA (solid line) and LDA+U (broken line) approaches. E_F is marked by the dotted line.

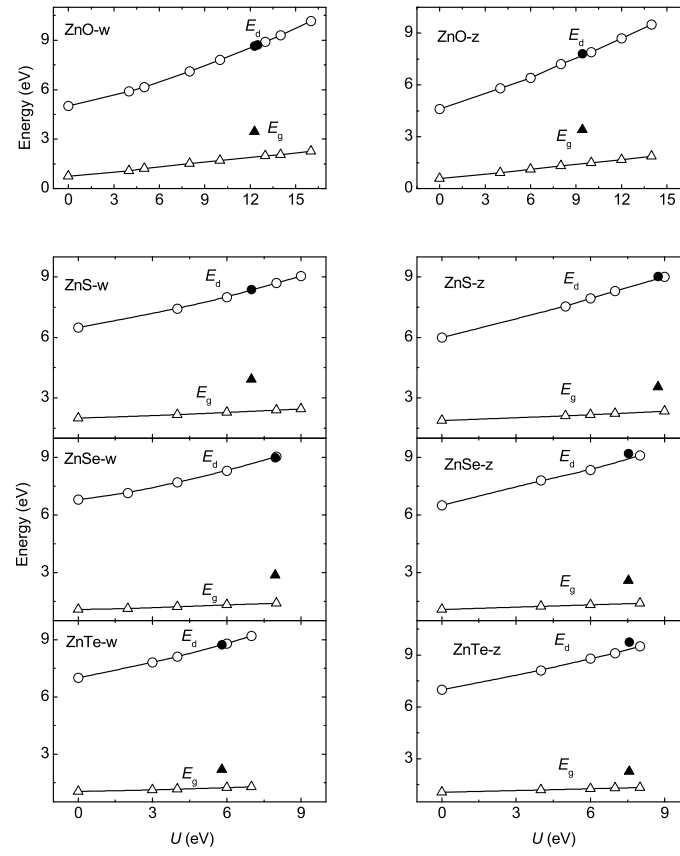


FIG. 3: Band gap (E_g) and mean energy level of the Zn-3d states (E_d) relative to the VB maximum for ZnX with z- and w-type structure as a function of the parameter U . Open symbols correspond to calculated data, and filled symbols are experimental data from Refs. 52,62,63,64. Due to the lack of experimental data for ZnO-z the experimental values for ZnO-w from Ref. 64 are used in the top right panel.

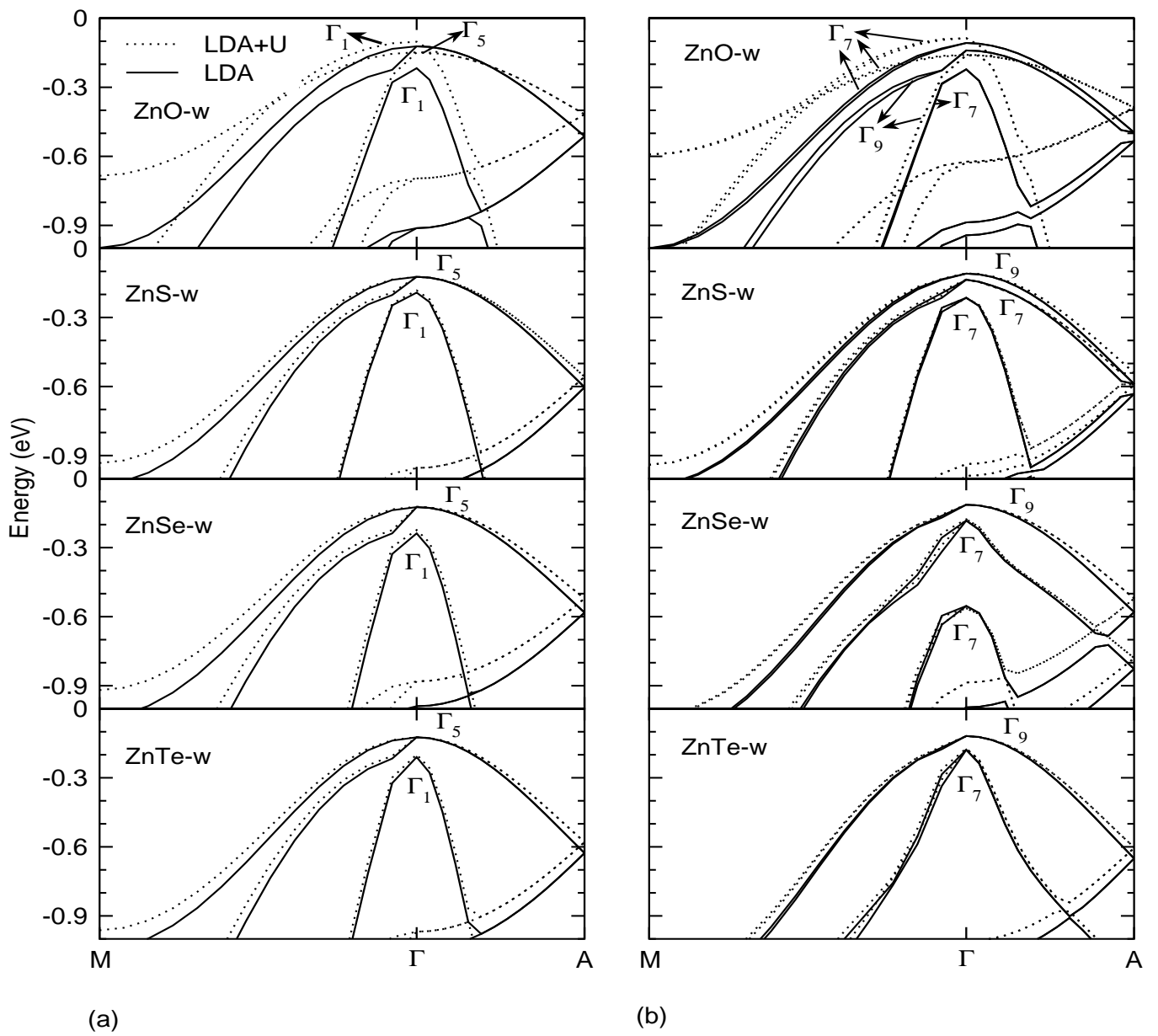


FIG. 4: Band structure of ZnX-w near the VBM maximum calculated by LDA (solid line) and LDA+U (dotted line) approaches: (a) neglecting and (b) including the SO coupling.

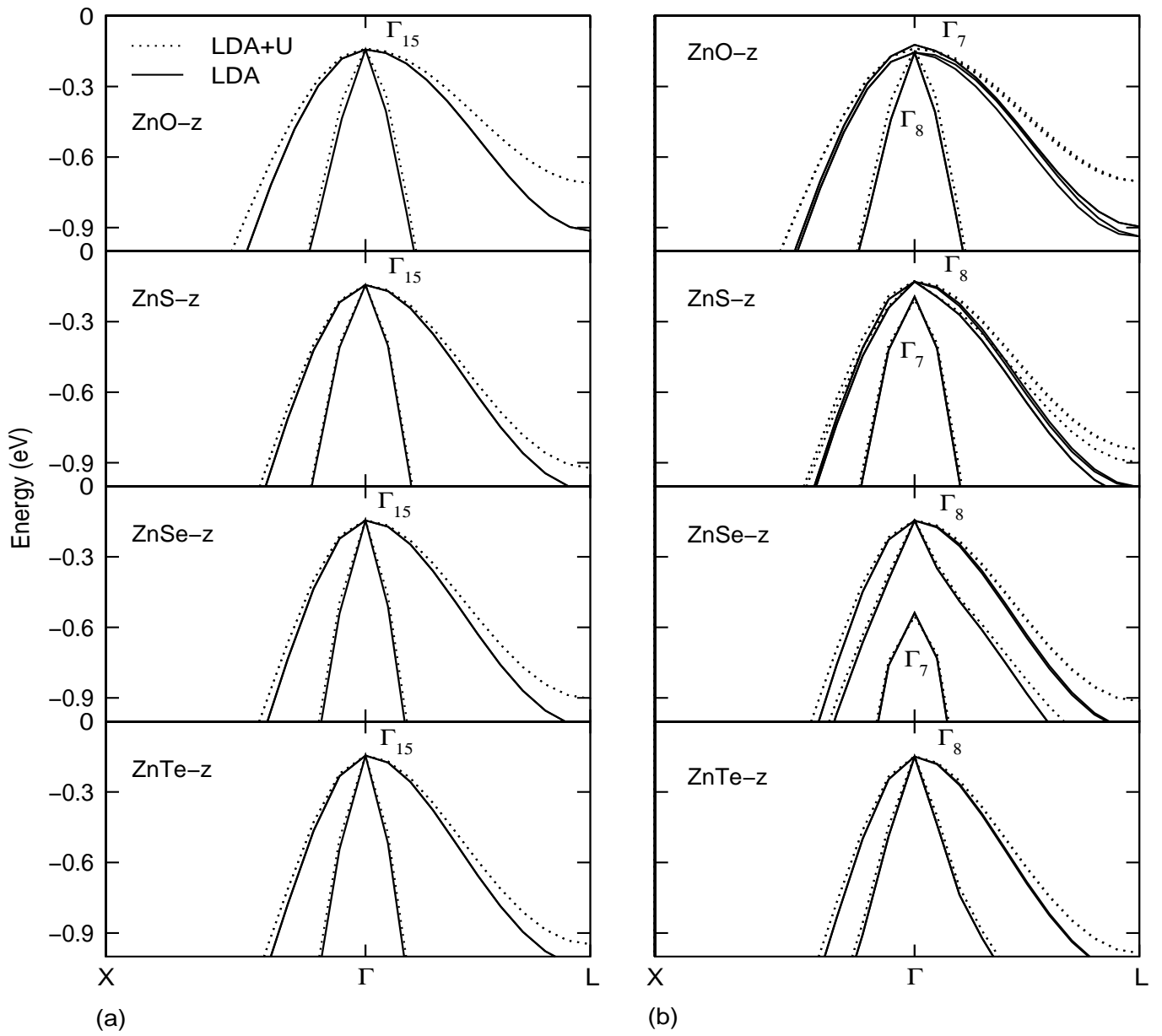


FIG . 5: Band structure for ZnX -z phases calculated by LDA (solid line) and LDA+U (dotted line) approaches: (a) neglecting and (b) including the SO coupling.

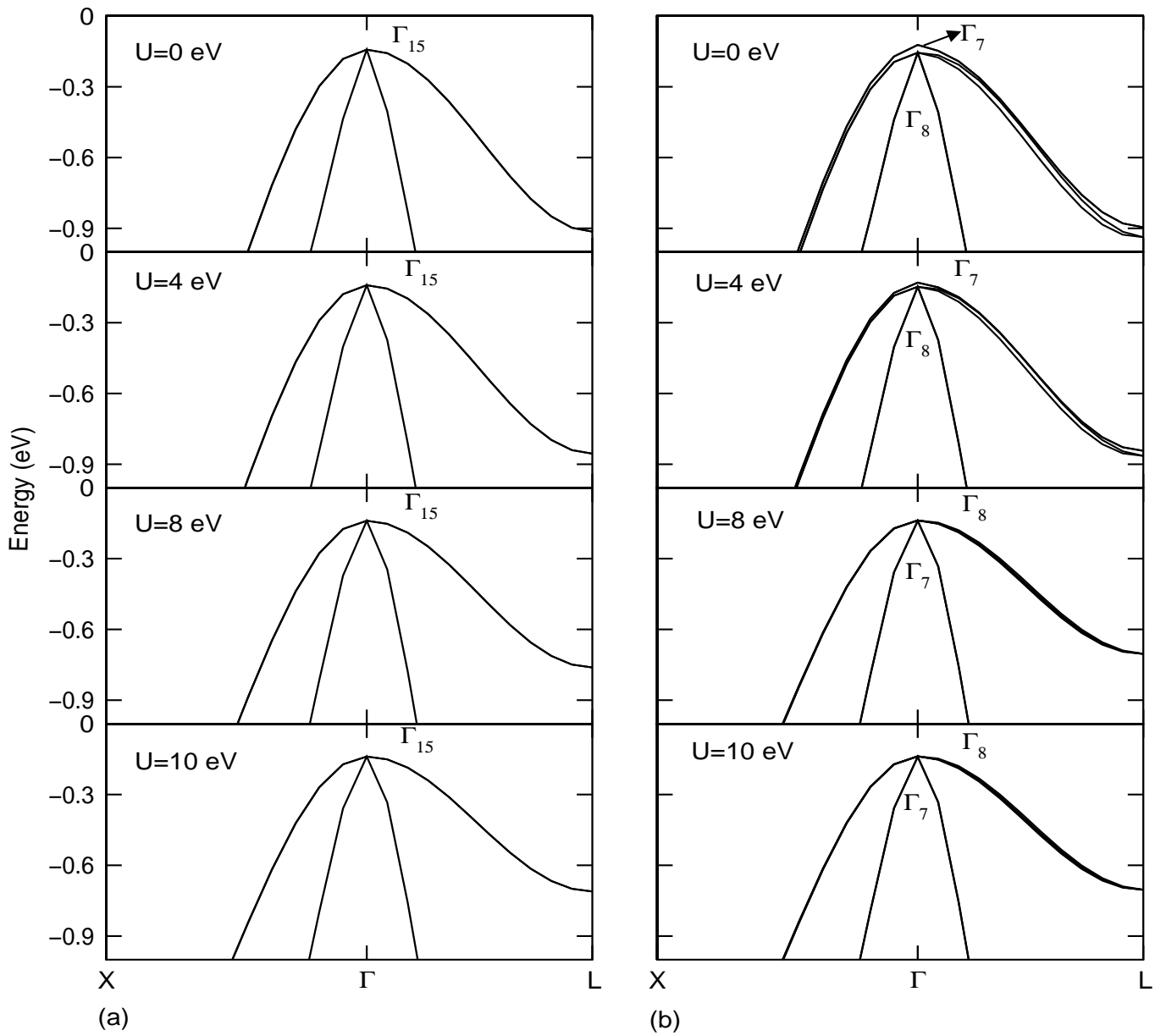


FIG .6: Evolution of the band structure of ZnO near the VB maximum with increasing the U : (a) neglecting and (b) including the SO coupling.

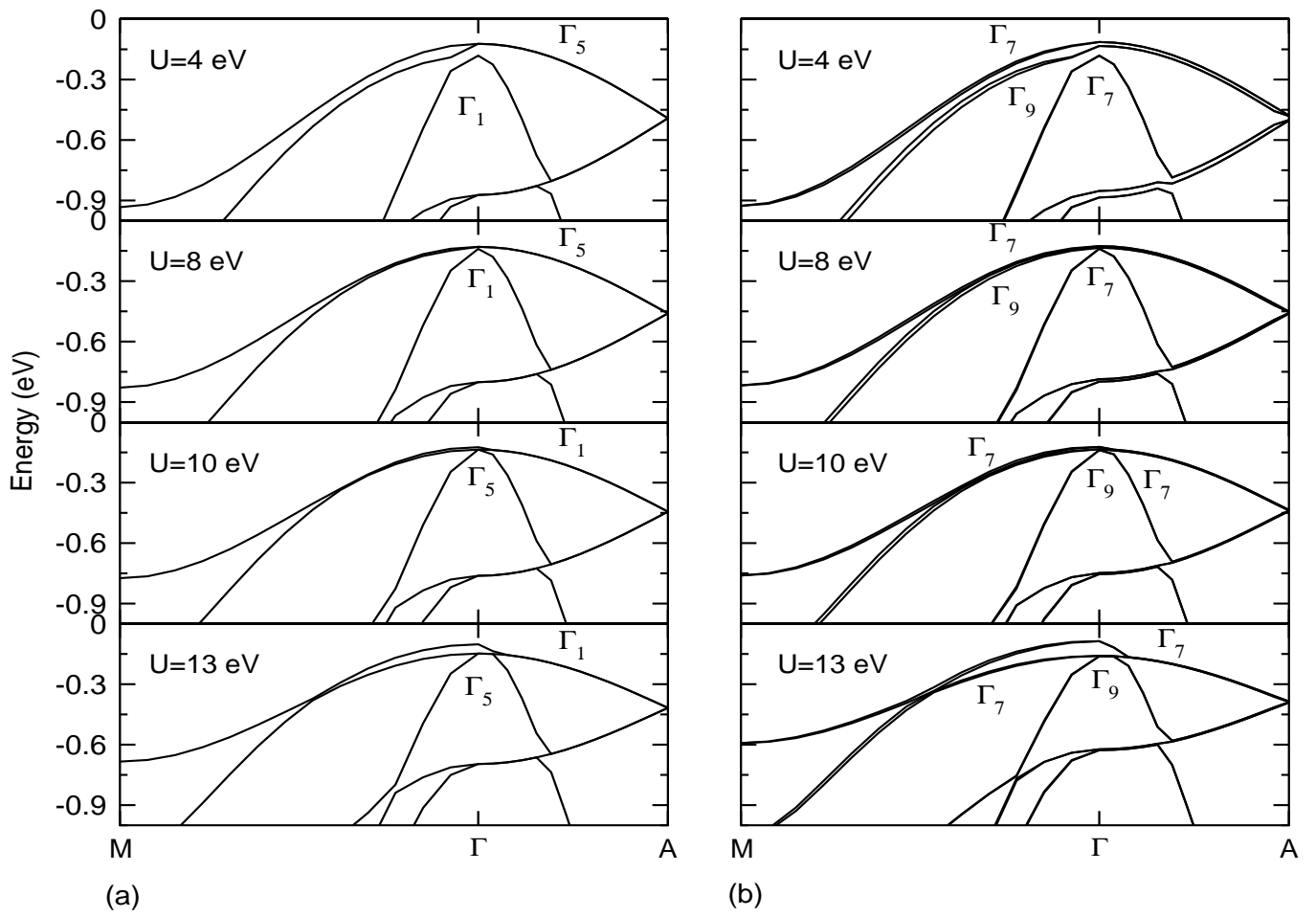


FIG . 7: Dependence of band structure of ZnO-w near the VB maximum on the parameter U : (a) neglecting and (b) including the SO coupling.

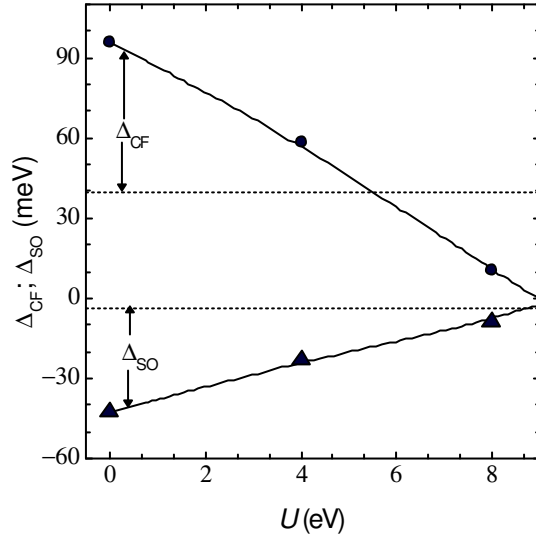


FIG. 8: Crystal-field and spin-orbit energy splitting as a function of U for ZnO-w. Solid and dotted lines represent calculated and experimental data, respectively.

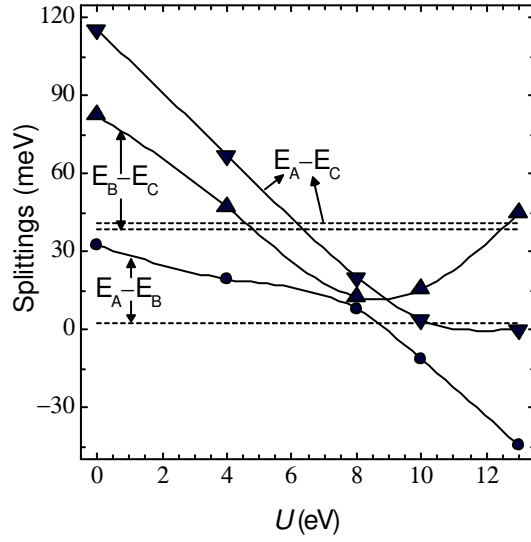


FIG . 9: Splitting of the states at the top of VB vs. U for ZnO-w . Solid and dotted lines represent calculated and experimental data, respectively.

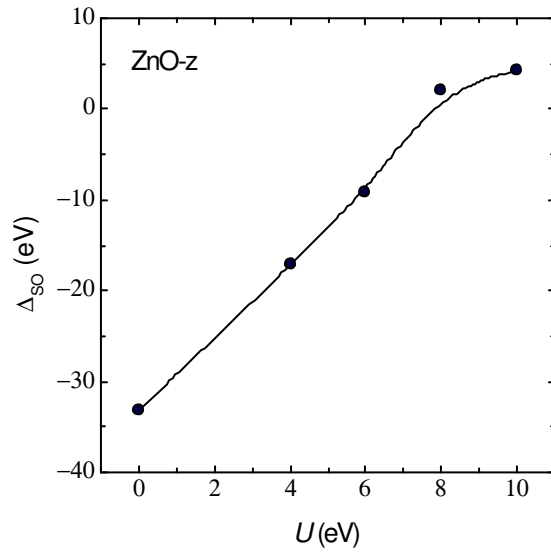


FIG . 10: Spin-orbit splitting energy for the zinc-blende ZnO .